PHYSICAL REVIEW B VOLUME 25, NUMBER 7 1 APRIL 1982

# Neutron-diffraction study of magnetically ordered $Tb_2Fe_3Si_5$

A. R. Moodenbaugh and D. E. Cox
*Physics Department, Brookhaven National Laboratory, Upton, New York 11973*

H. F. Braun*
*Institute for Pure and Applied Physical Sciences, University of California, San Diego, LaJolla, California 92093*

(Received 30 October 1981)

$Tb_2Fe_3Si_5$ has been studied by neutron-diffraction techniques at low temperatures. At 20 K the diffraction pattern is characteristic of the tetragonal crystal structure (space group $P4/mnc$, $a=10.43$ Å, $c=5.48$ Å). The atomic positional parameters have been determined by Rietveld refinement of the data. Magnetic-scattering peaks were observed just below 10.3 K, corresponding to the antiferromagnetic ordering temperature determined by susceptibility measurements. Two sets of magnetic-scattering peaks coexist from just below the ordering temperature to the lowest temperature studied, 4.55 K. These data can be accounted for with the following magnetic model. In both cases moments appear only on Tb atoms and are directed along [001]. Above 7 K the predominant set is incommensurate, consistent with a sinusoidal modulation along [001] of an antiferromagnetic structure consisting of ferromagnetic (001) sheets coupled antiparallel. Below 7 K the predominant set is commensurate with $a$ and $c$ parameters double those of the chemical cell. In this structure the four Tb moments within (001) squares are coupled parallel. Adjacent squares in the $a$ and $c$ directions are coupled antiparallel. Interpretation of the two sets of peaks may invoke either two physically separate phases or a linear superposition of the two proposed magnetic structures.

## I. INTRODUCTION

The relationship between magnetism and superconductivity has long attracted interest, and the recent discovery of ternary compounds exhibiting both superconducting and magnetic order has provided a new impetus in this area. The interaction between magnetism and superconductivity has so far been studied in three families of ternary compounds, the molybdenum chalcogenides, $M Mo_6X_8$ (Refs. 1–3) the rare-earth rhodium borides, $RRh_4B_4$ (Refs. 4–7) and the rare-earth rhodium stannides, $RRh_xSn_y$ with $x \simeq 1$ and $y \simeq 4$.[8] Neutron-diffraction techniques have proved to be of great value in elucidating the magnetic order in these materials.[9]

Recently another group of ternary compounds containing iron has been discovered with the general formula $R_2Fe_3Si_5$.[10–12] Several of these tetragonal silicides (space group $P4/mnc$) have been found to be superconducting. $Sc_2Fe_3Si_5$, $Y_2Fe_3Si_5$, and $Lu_2Fe_3Si_5$ have transition temperatures of 4.5, 2.4, and 6.0 K, respectively.[13] Although Fe usually carries a moment in its compounds, Mössbauer-effect measurements indicate that Fe has no moment in compounds with this structure.[14,15]

When the rare-earth atom is magnetic, suspectibility measurements show that the resulting compound orders magnetically. In this paper we present the results of a neutron-diffraction study of antiferromagnetic $Tb_2Fe_3Si_5$. $Tb_2Fe_3Si_5$ has a paramagnetic moment $\mu_{\text{eff}}=9.6\mu_B$ per Tb ion and a Néel temperature of 10.3 K.[12,15] The ordering of the Tb moments is described in detail as a function of temperature, while the Fe is found to carry no moment, in agreement with the Mössbauer studies.[14,15]

## II. SAMPLE PREPARATION AND EXPERIMENT

Two $Tb_2Fe_3Si_5$ samples were prepared, each of approximate mass 4 g. Each sample was arc melted, annealed for 2 d at 1200 °C, 2 d at 1000 °C, and 2 d at 800 °C. Micrographs showed up to 2 vol. % of an impurity phase. The two samples were crushed, mixed together, and compressed into a pellet. The resulting sample was transferred to a cylindrical aluminum sample holder and mounted inside a liquid-helium cryostat.

The neutron-diffraction experiments were carried out at the Brookhaven National Laboratory High Flux Beam Reactor using a pyrolytic graphite monochromator. Higher-order contamination was suppressed with a pyrolytic graphite filter. Full scans were taken with 2.461-Å neutrons of $Tb_2Fe_3Si_5$ at 4.9, 8.9, and 20 K. For these the experimental arrangement consisted of a monochromator set for the

(002) reflection and a pyrolytic graphite analyzer set for (004). Collimation was set at 20′, 40′, 40′, and 20′ for in pile, monochromator sample, sample analyzer, and analyzer detector, respectively. Additional scans of $Tb_2Fe_3Si_5$ at 7.1 and 16 K were later performed with 2.385-Å neutrons. In this case the analyzer was set for the 002 reflection with the other features unchanged.

Several additional partial scans below 10.3 K were performed using both experimental setups. Rietveld profile analysis[16–18] was performed on the 20-K data to determine the structural parameters. A similar analysis was performed on the 4.9-K data to refine the model for the commensurate magnetic structure. Integrated magnetic intensities were used for analysis of the incommensurate pattern obtained at 8.9 K.

## III. RESULTS AND DISCUSSION

We first describe the general character of the neutron-diffraction patterns observed as a function of temperature before attempting to analyze diffraction data using specific models. At 20 K, above the ordering temperature $T_N$, nuclear-diffraction peaks are characteristic of $Tb_2Fe_3Si_5$ (Fig. 1, top). The lattice parameters are $a = 10.413$ Å, $c = 5.475$ Å, compared with room-temperature values determined from x-ray diffraction of $a = 10.43$ Å and $c = 5.48$ Å. No trace of any impurity phase was observed.

Scans over the angular region $2\theta = 12–18°$ taken with 2.461-Å neutrons show the evolution of the magnetic diffraction pattern below 10.3 K (Fig. 2). At 10.3 K, just above $T_N$, there are no peaks in this segment, but a very broad hump attributed to critical scattering exists. At 10.0 K a magnetic peak is apparent at $2\theta \approx 14°$. This peak cannot be indexed in terms of the chemical cell or any simple multiple of this. The peak is, however, near the position predicted for the (100) peak, $2\theta = 13.57°$, and in fact, corresponds to an incommensurate structure. Another magnetic peak, at $2\theta = 16°$, is just visible at 10 K. This peak represents a commensurate cell with lattice parameters double those of the chemical cell. This

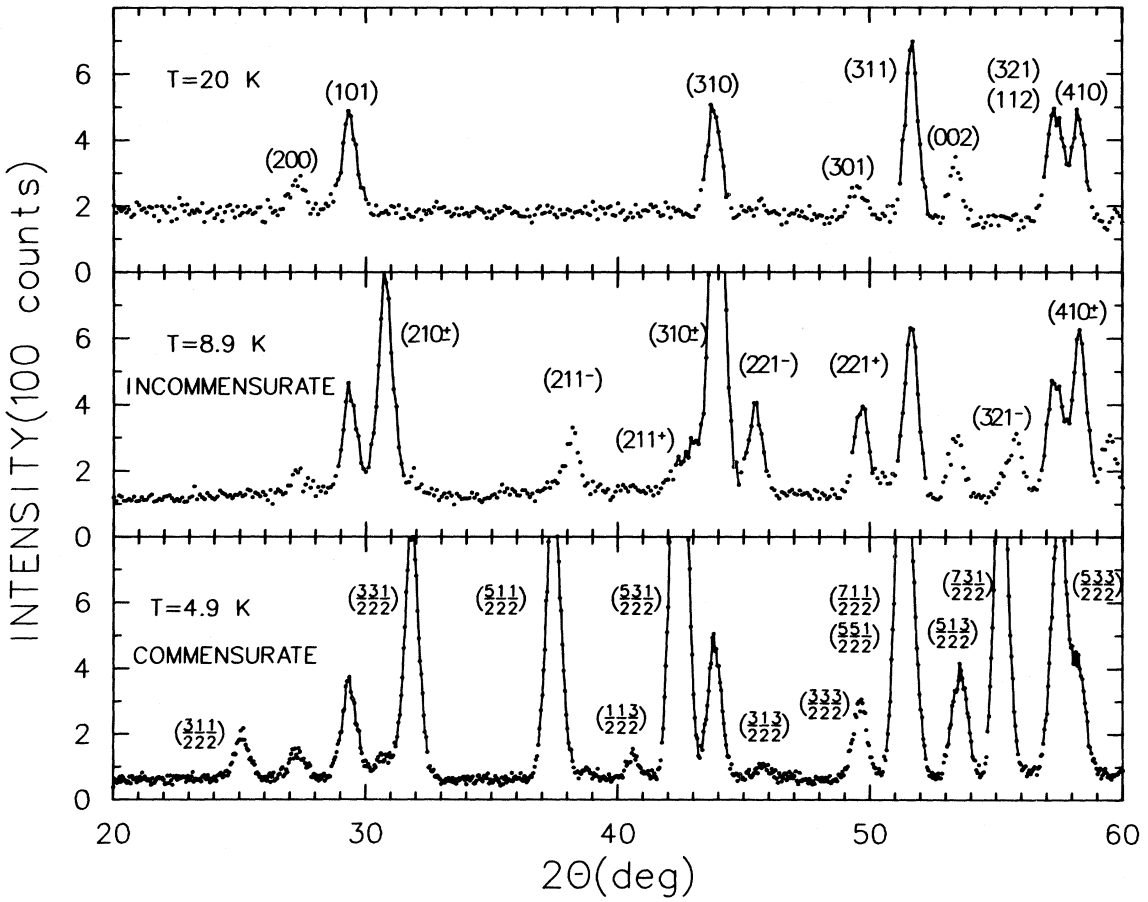


FIG. 1. Portions of three neutron-diffraction scans of $Tb_2Fe_3Si_5$, neutrons of 2.461 Å in each case. Major nuclear peaks are identified for 20-K data while major magnetic peaks are identified for 8.9- and 4.9-K data.

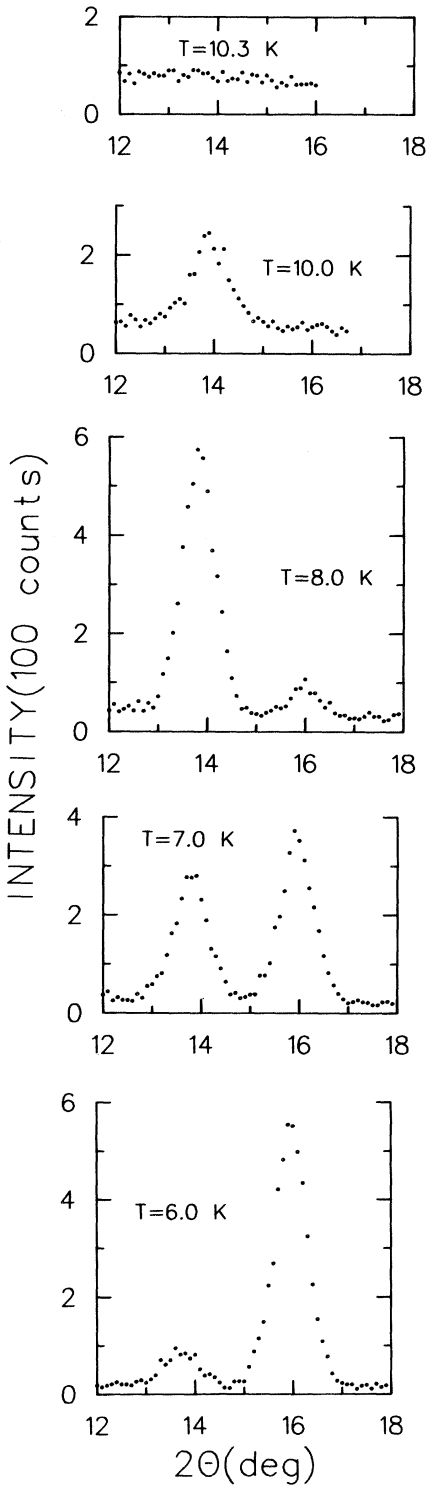


FIG. 2. Portions of neutron-diffraction scans (2.461 Å) illustrating the evolution of the commensurate and incommensurate magnetic patterns below 10.3 K. The peak near $2\theta = 14°$ represents the incommensurate pattern (identified as $100^{\pm}$; see text). The peak near $2\theta = 16°$ represents the commensurate pattern ($\frac{1}{2}\frac{1}{2}\frac{1}{2}$ peak).

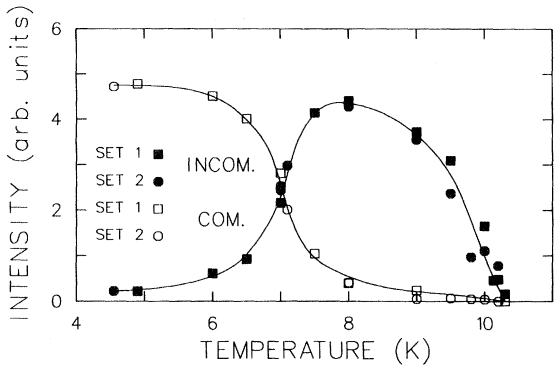


FIG. 3. Relative intensity vs temperature of incommensurate (INCOM.) and commensurate (COM.) peak intensities as represented by the $(100)^{\pm}$ and ($\frac{1}{2}\frac{1}{2}\frac{1}{2}$) peaks, respectively. Set 1 is from 2.461-Å data. Set 2, from 2.385-Å data, was normalized before plotting.

particular peak is indexable as the ($\frac{1}{2}\frac{1}{2}\frac{1}{2}$) peak in terms of the latter cell. Figure 3 shows the temperature dependence of intensity of these magnetic peaks.

As the temperature is reduced the incommensurate peak near $2\theta = 14°$ first increases in intensity, then begins decreasing near $T = 8$ K. A representative scan (Fig. 1, middle) at 8.9 K shows a larger portion of the pattern in this region. By about 7 K the commensurate ($\frac{1}{2}\frac{1}{2}\frac{1}{2}$) peak is more intense than the incommensurate peak. Below 7 K the commensurate structure predominates, but the incommensurate peaks do not completely disappear down to 4.55 K, the lowest temperature attained. A portion of a scan at 4.9 K is shown in Fig. 1, bottom. Note also that, as the temperature is reduced, the incommensurate peak shifts to a noticeably lower $2\theta$, i.e., closer to the position expected for the (100) peak at $2\theta = 13.57°$. No such shifts are observed for the commensurate or nuclear peaks.

### A. "Rietveld" refinement of structure from 20-K data

The neutron-diffraction data for $Tb_2Fe_3Si_5$ at 20 K were fitted by refinement of the structure using the Rietveld profile method.[16–18] For the refinement atomic positions were initially assigned the values published for the $Sc_2Fe_3Si_5$.[11] Lattice parameters were assigned estimated values and the overall temperature factor was initially set to zero. Regions of the scan which included peaks due to scattering from the aluminum sample container were excluded from consideration. Neutron cross sections were taken from the compilation of Koester.[19] The results of the refinement are collected in Table I. The fit of the calculated curve to the data is shown in Fig. 4. The

TABLE I. Parameters from Rietveld refinement. $U$, $V$, $W$ are half-width parameters (Refs. 16 and 17) $R_I$, $R_{WP}$, and $R_E$ are $R$ factors defined by Hewat (Ref. 18) for integrated intensities, weighted profile and statistical, or expected values. Estimated standard deviations (esd's) are given in parentheses based on the least significant figure. Values fixed initially have no esd indicated. Esd's quoted for $a$ and $c$ do not take into account any uncertainty in the neutron wavelength.

| Parameter | | $T=20$ K | $T=4.9$ K |
|---|---|---|---|
| Tb, 8($h$): | $x$ | 0.0698(4) | 0.0690(4) |
| | $y$ | 0.2352(5) | 0.2336(6) |
| | $z$ | 0 | 0 |
| $Fe_1$, 8($h$): | $x$ | 0.3770(4) | 0.3734(5) |
| | $y$ | 0.3555(4) | 0.3560(6) |
| | $z$ | 0 | 0 |
| $Fe_2$, 4($d$): | $x$ | 0 | 0 |
| | $y$ | $\frac{1}{2}$ | $\frac{1}{2}$ |
| | $z$ | $\frac{1}{4}$ | $\frac{1}{4}$ |
| $Si_1$, 8($g$): | $x$ | 0.1770(6) | 0.1741(11) |
| | $y$ | 0.6770(6) | 0.6741(11) |
| | $z$ | $\frac{1}{4}$ | $\frac{1}{4}$ |
| $Si_2$, 4($e$): | $x$ | 0 | 0 |
| | $y$ | 0 | 0 |
| | $z$ | 0.2587(22) | 0.2597(44) |
| $Si_3$, 8($h$): | $x$ | 0.1830(8) | 0.1751(19) |
| | $y$ | 0.4776(9) | 0.4840(12) |
| | $z$ | 0 | 0 |
| Tb moment ($\mu_B$) | | . . . | 8.60(5) |
| Temp. factor $B$ (Å$^2$) | | −0.66(10) | 0.55(20) |
| $a$ (Å) | | 10.4132(8) | 10.4088(10) |
| $c$ (Å) | | 5.4747(5) | 5.4737(5) |
| $U$ (deg$^2$) | | 0.82(6) | 0.41(22) |
| $V$ (deg$^2$) | | −1.12(10) | −0.68(23) |
| $W$ (deg$^2$) | | 0.75(5) | 0.64(6) |
| Zero point (deg) | | −0.057(6) | −0.077(6) |
| $R_I$ (%) | | 8.4 | 5.0 |
| $R_{WP}$ (%) | | 15.4 | 7.9 |
| $R_E$ (%) | | 11.8 | 5.0 |

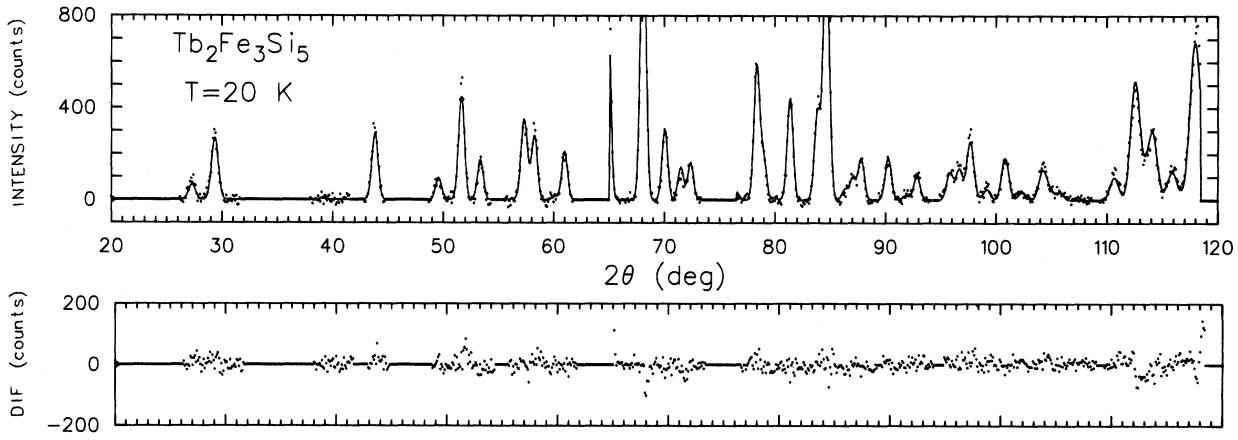


FIG. 4. Rietveld profile fit to 20-K data. Observed counts are data points. Calculated intensities are connected by the line. DIF. is the difference between observed counts and calculated counts. Estimated background is subtracted from raw data. DIF. is zero in excluded regions and in regions in which no peak is predicted.

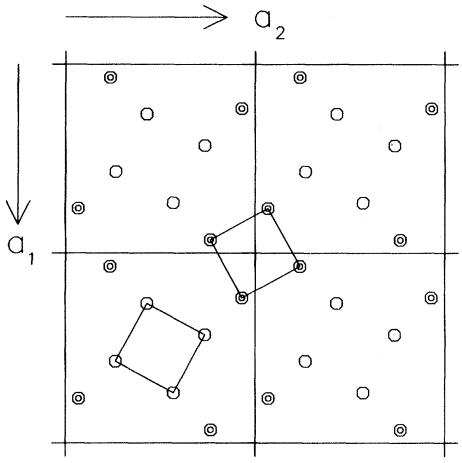


FIG. 5. Illustration of Tb positions in four adjacent chemical cells. View is along [001]. Cell edges are straight lines. Tb atoms at $z=0$ are shaded symbols; Tb atoms at $z=c/2$ are open symbols.

lattice parameters, $a=10.413$ Å and $c=5.475$ Å are somewhat lower than those found at room temperature by x-ray diffraction, $a=10.43$ Å and $c=5.48$ Å.[15] the $R_I$ factor, which is based on integrated intensities, is 8.4%. The weighted profile value $R_{WP}=15.4\%$ (based on weighted point-by-point data) can be compared with the statistical or expected $R_E$ of 11.8%. The isotropic temperature factor $B$ determined in this refinement is negative. There is no apparent explanation for this; however, such results are not uncommon when applying Rietveld refinement and do not appear to invalidate the positional parameters determined in the refinement.

To facilitate description of the magnetic structure, it is desirable at this point to describe the positions of Tb atoms in the cell. Figure 5 illustrates these projected on the (001) plane. The solid lines define chemical unit-cell edges of length $a=10.413$ Å. Shaded circles are Tb atoms at $z=0$ and open circles are Tb atoms at $z=0.5$ along the $c$ axis. The Tb atoms form near-neighbor squares in the planes at these heights, two per cell, about 3.60 Å on a side.

### B. Magnetic scattering at 8.9 K

Part of the data taken at 8.9 K is displayed in Fig. 1 (center). At this temperature the incommensurate peaks have attained about 80% of their maximum values. In contrast, the commensurate magnetic peaks which dominate below 7 K contain less than 10% of the total coherent magnetic intensity.

The peak positions of the incommensurate component can all be accounted for on the basis of a modulation along the [001] direction such that $d^{*2}$ is given by the equation

$$d^{*2}=(h^2+k^2)a^{*2}+(l\pm\delta)^2c^{*2}\ , \tag{1}$$

where $\delta=c/\lambda_I\approx 0.135$, $\lambda_I$ being the wavelength of the modulation.[20] For $l=0$, the value of $d^{*2}$ differs from that of a commensurate peak [e.g., (210), (310), and (410) in Fig. 1, center] by only second order in $\delta$. Then only one peak (denoted $hk0\pm$) is predicted to appear on the high-angle side of the corresponding ($hk0$) peak position. However for $l\neq 0$, the spacing equation is first order in $\delta$, and two peaks (denoted $hkl^-$ and $hkl^+$) are predicted to occur nearly symmetrically about the corresponding commensurate position ($hkl$). This situation is illustrated in Fig. 1, center, by the $(211^-)$, $(211^+)$ and $(221^-)$, $(221^+)$ pairs.

The proposed model contains the following features. First, Tb moments are the sole contributors to the magnetic scattering. This is plausible since the Mössbauer-effect results indicate that the iron atoms have no moment.[14,15] The absence of magnetic peaks ($00l$) suggests the Tb moments are directed along [001]. In the model all Tb moments within an (001) plane are parallel along the [001] direction, and atoms at $z=0$ have moments directed antiparallel to those at $z=0.5$. In addition the amplitude of the moments is modulated by a sinusoidal incommensurate wave directed along [001], with a period of about $7.4c$. Thus the structure consists of ferromagnetic (001) planes which are stacked alternately, with an additional incommensurate sinusoidal amplitude modulation of the moment along [001].

Relative intensities of the magnetic peaks were calculated for the proposed model using calculated spherical form factors for Tb.[21] Integrated intensities for the incommensurate phase were determined by subtraction of overlapping contributions from the nuclear and commensurate magnetic peaks where appropriate. Table II contains a list of calculated and observed peak positions for well-resolved peaks, and normalized calculated and observed magnetic intensities for peaks below $2\theta=60°$ using $\delta=0.135$ ($\lambda_I=7.4c$), $a=10.4132$ Å and $c=5.4747$ Å. Observed positions were corrected for a zero-point error of $2\theta=0.06°$ obtained from the Rietveld refinement of 20-K data. Agreement between calculated and observed intensities is reasonably good, particularly in view of the many overlapping peaks which interfere with the accurate determination of the experimental peak intensities. Omitted from Table II are peaks with $h+k+l=2n$ and with $h=k$ or $h=0$ or $k=0$. A selection rule for the proposed model predicts these peaks to be absent, and none is in fact observed. Also omitted are peaks of the form $00l$ since none is observed. The model predicts these to be absent because the scattering vector is parallel to the

TABLE II. Incommensurate peaks ($2\theta < 60°$) relative intensities and positions compared with calculated values. Observations were taken from 8.9-K data. Some peaks are omitted from observed data list because they are obscured by nuclear peaks. See text for details.

| | Position $2\theta$ (deg) | | Intensity (arb. units) | |
|---|---|---|---|---|
| *hkl* | Calc. | Obs. | Calc. | Obs. |
| $100^{\pm}$ | 14.02 | 13.94 | 1000 | 1200 |
| $111^{-}$ | 29.72 | | 5 | |
| $210^{\pm}$ | 30.86 | 30.84 | 523 | 434 |
| $111^{+}$ | 35.52 | | 3 | 24 |
| $201^{-}$ | 35.65 | | 17 | |
| $211^{-}$ | 38.31 | 38.25 | 126 | 156 |
| $201^{+}$ | 40.71 | | 13 | |
| $300^{\pm}$ | 41.70 | | ~0 | |
| $211^{+}$ | 43.11 | | 101 | 115 |
| $310^{\pm}$ | 44.05 | | 662 | 607 |
| $221^{-}$ | 45.51 | 45.52 | 177 | 173 |
| $221^{+}$ | 49.74 | | 152 | |
| $311^{-}$ | 49.84 | | 12 | 161 |
| $320^{\pm}$ | 50.59 | | 52 | |
| $102^{-}$ | 51.64 | | 8 | |
| $311^{+}$ | 53.82 | | 10 | |
| $321^{-}$ | 55.87 | 55.87 | 137 | 126 |
| $410^{\pm}$ | 58.39 | | 126 | 143 |
| $102^{+}$ | 59.24 | | 6 | |
| $212^{-}$ | 59.42 | | 31 | 114 |
| $321^{+}$ | 59.57 | 59.57 | 123 | |

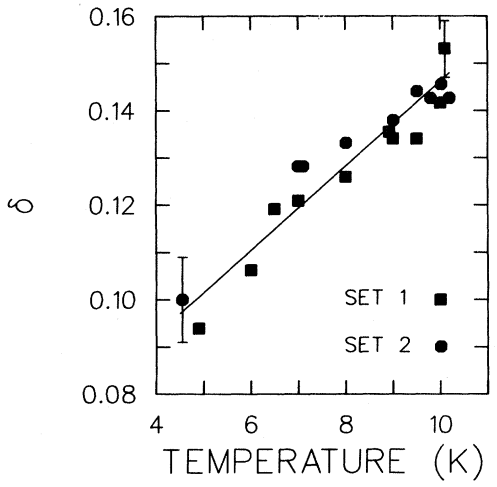


FIG. 6. Incommensurate modulation of Tb moments along [001], $\delta$, as a function of temperature. Straight line drawn through the data is a guide for the eye. Set 1 refers to points obtained from 2.461-Å neutron data; set 2, 2.385-Å neutrons. Data were obtained from position of $(100)^{\pm}$ peak at various temperatures. See Fig. 2 for examples. Representative error bars are obtained from an uncertainty in position of peak (estimated to be $\pm 0.04°$ in $2\theta$).

magnetic moment vector along [001], and hence the magnetic interaction vector amplitude $q$ is zero. Calculations made for peaks appearing out to $2\theta = 120°$ also agree well with the data.

The model discussed above includes the assumption that the incommensurate modulation is sinusoidal. Any departure from sinusoidal modulation of the moments would be accompanied by higher-order incommensurate satellites.[20] Such a satellite of the (100) peak, the $100^{3\pm}$, is calculated to appear at about $2\theta = 17.0°$ in the case of 2.461-Å neutrons. We estimate that scattering at that position would be apparent if it exceeded about 1% of the intensity of the $(100^{\pm})$ peak. No peak is observed in data taken at 7.1 and 8.9 K. This negative result can be compared with the prediction that, for a square wave, the third harmonic would be about 12% of the fundamental peak intensity.[20]

One final point is that the incommensurate modulation varies appreciably with temperature. This is shown in Fig. 6, in which $\delta$ as determined from the positions of the $100^{\pm}$ peak is plotted as a function of temperature.

### C. Magnetic scattering at 4.9 K

At 4.9 K the commensurate magnetic pattern accounts for about 95% of the coherent magnetic scattering (Fig. 1, bottom). Magnetic peaks are indexed relative to the chemical cell with half-integral values of $h$, $k$, and $l$.

The pattern was fitted by Rietveld refinement using magnetic peak intensities for the following uniaxial model. As in the case of the incommensurate model, Tb moments are the sole contributors to the magnetic scattering and are directed along the [001] axis. In addition all Tb moments in each near-neighbor square are directed in the same direction. However, in contrast to the incommensurate structure, the half-integral indices demand a reversal in the direction of a Tb moment following translation by one chemical cell length along any of the axes. These features fully describe the overall antiferromagnetic structure which is a three-dimensional "checkerboard," each unit being a square of Tb moments.

Results of Rietveld refinement are shown in Table I. The fit of the calculated curve to the data is shown in Fig. 7. Several regions of the pattern containing small residual magnetic contributions from the incommensurate pattern were excluded from consideration as well as regions containing scattering from the Al sample container. Preliminary values for parameters were estimated from the 20-K refinement, and an initial value of $8.0\mu_B$ was taken for the Tb moment. Good agreement is achieved between calculated and observed patterns, as shown by the various $R$ factors in Table I. $R_{WP}$ is 7.9% compared with the

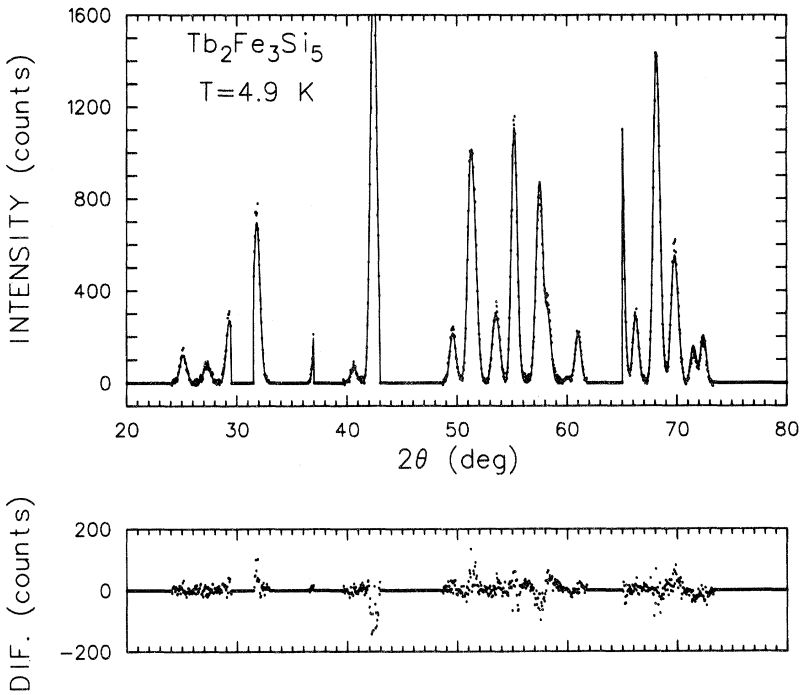


FIG. 7. Rietveld profile fit to 4.9-K data. Observed counts are data points. Calculated intensities are connected by the line. DIF. is the difference between observed counts and calculated counts. Estimated background is subtracted from raw data. DIF. is zero in excluded regions and in regions in which no peaks are predicted.

expected $R_E$ of 5.0%. In contrast to the 20-K result, the isotropic temperature factor $B$ determined in this refinement has a positive value.

The magnetic moment determined in the refinement is $\mu = 8.6\mu_B$. However, the calculated value must be corrected for the presence of a small amount of scattering from the incommensurate component. This correction, which depends on the specific model chosen to account for the appearance of the two sets of peaks at the same temperature, will be discussed in Sec. III D.

### D. Intermediate temperature region

In the above discussion we have analyzed the commensurate and incommensurate patterns in terms of separate magnetic structures. However, since the two sets of peaks coexist from near $T_N = 10.3$ down to 4.55 K, the lowest temperature reached, we must consider whether these two models actually correspond to two separate, coexisting physical phases (two phase hypothesis), or whether there is really only one phase over the whole temperature range (single-phase hypothesis). In the case of the single-phase hypothesis, since the direction of the moments is along the [001] axis for both commensurate and incommensurate models, the magnetic structure would have to be a linear superposition of Tb moments of the two models which describes magnetic ordering throughout the sample. There is no direct evidence from the neutron scattering results which might confirm either of these hypotheses, but we will discuss the results in relation to the hypotheses.

First, the two patterns coexist over virtually the complete temperature range in which magnetic ordering is observed. Such a broad range of coexistence would tend to favor the single-phase model, since, if two competing separate physical phases were to exist, the transition between the two states might be expected to occur over a relatively small temperature interval. In addition, we find no evidence of hysteresis in the data within the accuracy of observation, about 0.1 K. The lack of observed hysteresis also favors the single-phase hypothesis.

On the other hand, sample inhomogeneity could play a role in the coexistence of two phases over a broad range of temperature. This could make the two-phase hypothesis reasonable. However, there is no reason to believe there is any significant sample inhomogeneity. Certainly the good agreement of the profile fit utilizing the assumed atomic species and positions tends to argue against atomic disorder or gross deviations from stoichiometry. As a further check one might determine the sensitivity of the magnetic structure to changes in composition by studying the magnetic structure of samples prepared using different annealing programs and with different compositions.

The dependence on temperature of the maximum magnetic moment of a Tb atom $\mu_{Tb}$ depends on the hypothesis chosen. For the two-phase hypothesis the magnetic moment cannot be uniquely determined from neutron-diffraction results. The equations for incommensurate and commensurate peak intensities ($I_I$ and $I_C$) are

$$I_I = Cf_I\mu_I^2 k_I, \quad I_C = C(1-f_I)\mu_C^2 k_C \ , \tag{2}$$

where $C$ is an instrumental scale factor, $f_I$ is the fraction of the sample with incommensurate structure, $\mu_I$ and $\mu_C$ are the respective Tb moments of the incommensurate and commensurate phases at a given temperature, and $k_I$ and $k_C$ are known quantities for each peak (assuming the correctness of the incommensurate and commensurate models). If it is assumed that $\mu_I = \mu_C = \mu_{Tb}$, $f_I$ can be determined and $\mu_{Tb}$ can be calculated for temperatures between 4.55 and 10.2 K. The value of the Tb moment at 4.9 K, where the Rietveld fit of the complete pattern determines $\mu_C$ to an accuracy of about $\pm 0.2\mu_B$, is $8.7\mu_B$, after making a small correction (about $+0.1\mu_B$) to allow for the assumption made in the Rietveld calculation that the commensurate phase is the only one present throughout the sample. This value $\mu_{Tb} = 8.7\mu_B$ is in good agreement with the Tb saturation moment of $9\mu_B$. The ratio $I_I/I_C$ was determined at 4.9 K and other temperatures from the ratio of the intensities of the $(100)^{\pm}$ and $(\frac{1}{2}\frac{1}{2}\frac{1}{2})$ peaks (several examples are shown in Fig. 2). Figure 8 shows the maximum Tb moment versus temperature as determined by the above method for the two-phase hypothesis.

For the single-phase hypothesis $\mu_{Tb}$ is determined without any further assumptions. Here

$$I_I = C\mu_I^2 k_I, \quad I_C = C\mu_C^2 k_C \ , \tag{3}$$

where the definitions are those of the preceeding paragraph. In this case the maximum moment $\mu_{Tb} = \mu_I + \mu_C$. The $\mu_C$ determined at 4.9 K was again used as a basis for the calculation. In this case no correction is applied to $\mu_C$ since this hypothesis assumes, as does the Rietveld calculation, that the commensurate phase exists throughout the sample. Figure 8 shows the maximum Tb moment plotted against temperature. A distinct maximum in the moment appears near 7 K. The maximum Tb moment calculated assuming the single-phase hypothesis is significantly greater than the Tb saturation moment of $9\mu_B$. Thus the two-phase hypothesis predicts a more typical dependence of $\mu_{Tb}$ on temperature.

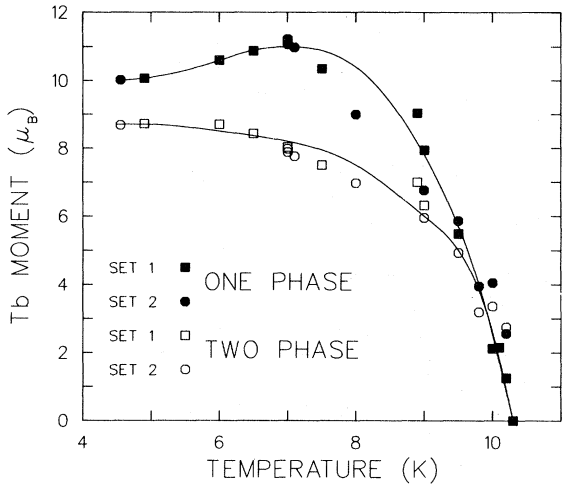


FIG. 8. Maximum magnetic moment, $\mu_{Tb}$ vs temperature for two cases. Filled symbols represent the single-phase hypothesis. Open symbols represent results for the two-phase hypothesis with the additional assumption that the maximum Tb moments in each phase are equal to each other. See text for details. Set 1 from 2.461-Å neutron results; set 2 from 2.385-Å neutron results. Lines drawn through the data are a guide for the eye.

One final point to be noted is that electrical resistivity[22] and magnetic susceptibility[12,15] measurements show unusual behavior near 7 K, the temperature at which there is the greatest rate of change between the incommensurate and commensurate patterns.

## ACKNOWLEDGMENTS

The authors thank S. M. Shapiro for a critical reading of the manuscript and many helpful suggestions. Work performed at BNL is supported by the U.S. Department of Energy under Contract No. DE-AC02-76CH00016. Work performed at UCSD is supported by the National Science Foundation Grant No. NSF/DMR77-08469.

*Current address: Dépt. de Phys. de la Matière Condensée, Université de Genève, Genève 4, Switzerland.

[1]Ø. Fischer, A. Treyvaud, R. Chevrel, and M. Sergent, Solid State Commun. 17, 721 (1975).
[2]M. Ishikawa and Ø. Fischer, Solid State Commun. 24, 747 (1977).
[3]R. N. Shelton, R. W. McCallum, and H. Adrian, Phys. Lett. 56A, 213 (1976).
[4]J. M. Vandenberg and B. T. Matthias, Proc. Natl. Acad. Sci. U.S.A. 74, 1336 (1977).
[5]B. T. Matthias, E. Corenzwit, J. M. Vanderberg, and H. Barz, Proc. Natl. Acad. Sci. U.S.A. 74, 1334 (1977).
[6]W. A. Fertig, D. C. Johnson, L. E. DeLong, R. W. McCallum, M. B. Maple, and B. T. Matthias, Phys. Rev. Lett. 38, 987 (1977).
[7]D. C. Johnston, Solid State Commun. 24, 699 (1977).

[8]J. P. Remeika, G. P. Espinosa, A. S. Cooper, H. Barz, J. M. Rowell, D. B. McWhan, J. M. Vanderberg, D. E. Moncton, Z. Fisk, L. D. Woolf, H. C. Hamaker, M. B. Maple, G. Shirane, and W. Thomlinson, Solid State Commun. 34, 923 (1980).

[9]For a recent review of neutron-diffraction studies, see W. Thomlinson, in *Superconductivity in Ternary Compounds,* Topics in Current Physics, edited by Ø. Fischer and M. B. Maple (Springer-Verlag, Berlin, in press).

[10]O. I. Bodak, V. K. Pecharskii, and E. I. Gladyshevskii, Izv. Acad. Nauk SSSR, Neorg. Mater. 14, 250 (1978) [Inorg. Mater. (USSR) 14, 188 (1978)].

[11]O. I. Bodak, B. Ya. Kotur, V. I. Yarovets, and E. I. Gladyshevskii, Kristallografiya 22, 385 (1977) [Sov. Phys. Crystallogr. 22, 217 (1977)].

[12]H. F. Braun, in *Ternary Superconductors,* edited by G. K. Shenoy, B. D. Dunlap, and F. Fradin (Elsevier–North-Holland, New York, 1981), p. 225.

[13]H. F. Braun, Phys. Lett. 75A, 386 (1980).

[14]J. D. Cashion, G. K. Shenoy, D. Niarchus, P. J. Viccaro, and Charles M. Falco, Phys. Lett. 79A, 464 (1980).

[15]H. F. Braun, C. U. Segre, F. Acker, M. Rosenberg, S. Dey, and P. Deppe (unpublished).

[16]H. M. Rietveld, Reactor Centrum Nederland Research Report No. RCN 104 (unpublished).

[17]H. M. Rietveld, J. Appl. Crystallogr. 2, 65 (1969).

[18]A. W. Hewat, Atomic Energy Authority Research Group Report No. RRL 73/897 (unpublished).

[19]L. Koester, in *Springer-Verlag Tracts in Modern Physics,* edited by G. Hoehner (Springer-Verlag, Berlin, 1977), Chap. 8.

[20]G. E. Bacon, *Neutron Diffraction,* 3rd ed. (Clarendon, Oxford, 1975), Chap. 8.

[21]M. Blume, A. J. Freeman, and R. E. Watson, J. Chem. Phys. 37, 1245 (1962).

[22]H. F. Braun (unpublished).